Detection of inhibitory effects in the generation of breakdown spots in HfO_2-based MIM devices

J. Muñoz-Gorriz[1], S. Monaghan[2], K. Cherkaoui[2], J. Suñé[1], P.K. Hurley[2], E. Miranda[1]

[1]Departament d'Enginyeria Electrònica, Universitat Autònoma de Barcelona, Spain

[2]Tyndall National Institute, University College Cork, Cork, Ireland

E-mail address of corresponding author: jordi.munoz.gorriz@uab.cat

Abstract

In this work, the connection between the generation of catastrophic breakdown (BD) spots in metal-insulator-metal capacitors with a high-permittivity dielectric film (HfO_2) and their spatial distribution was investigated. To gain insight into this issue, large area devices (10^4 μm^2) were constant voltage stressed at high electric fields (3.5 MV/cm) with the aim of generating a large number of spots in a single device. The set of BD spots was analysed as a point pattern with attributes (their sizes) using the methods of spatial statistics. Our study reveals that beyond the visible damage on the top metal electrode, the spots exhibit soft-inhibition regions around them where the creation of new spots is less likely. The origin of these inhibitory regions is ascribed to structural modifications of the dielectric layer in the vicinity of the spots caused by the huge thermal effects occurring at the very moment of the BD event.

Keywords: oxide breakdown; reliability, MIM, spatial statistics

1. Introduction

When electrically stressed, defects are randomly generated within the insulating layer of capacitor-like devices such as metal-insulator-metal (MIM) and metal-insulator-semiconductor (MIS) structures. This generation of defects ultimately leads to the destruction of the device because of the formation of a short across the dielectric that enables an uncontrolled flow of electrons between the top and the bottom electrodes (see Fig. 1). Since this process is associated with Joule heating effects, a huge amount of thermal energy is dissipated in a very tiny area, producing a local microexplosion of the film with the consequent evaporation of the electrodes. This event is often referred to as hard or catastrophic breakdown (BD) and is linked to irreversible changes in the physical and electric properties of the devices [1]. The final result is the appearance of a mark on the top metal layer visible by means of an optical microscope [2]. The study of this kind of phenomenon (time-to-BD, localization of failure sites, etc.) is crucial for a given technology since it provides valuable information about its reliability aspects [3].

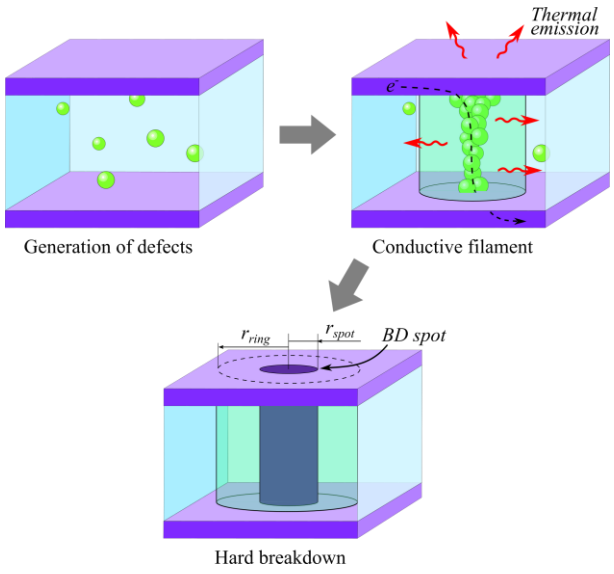

Figure 1. Schematic representation of the BD spot generation. First, defects are randomly generated within the dielectric layer. Then a percolation path is formed, and a high thermal energy is released. Finally, the top electrode melts leaving a mark on the metal plate.

The study of the BD phenomenon in oxide films usually involves electrical measurements exclusively and relies on the analysis of the generation of single BD events in a large set of devices. However, in previous works we showed that when multiple events are observed in a single device, spatial statistics provides suitable methods for characterizing the spatial distribution of the damage occurring both in MIM and MIS structures [2], [4], [5]. In the case of large area devices, it is possible to have a large number of BD spots per device so that the set of marks can be collectively treated as a point pattern (position) with attributes (size). The connection between the location and the attribute can also be investigated using the methods of spatial statistics [6]. Very often a Poisson or complete spatial randomness (CSR) model is assumed for the distribution of marks over the structure area. This is consistent with the Weibull-type time-to-failure distribution obtained from a large number of small area devices. In this work, we have investigated up to what extend the hypothesis of CSR holds for severely damaged devices. To this end, devices with large area (10^4 μm^2) and high electric fields (3.5 MV/cm), like the ones used in this work are imperatively required. Deviations from a CSR distribution would indicate that the generation of BD spots is not completely random [7]. Recall that this is not only a problem related to the dimensions of the observation area but also to the density of spots in that area. In addition, not only the location of the spots was investigated in this work but also their sizes. This kind of analysis requires high accuracy in the determination of the location of the BD event as well as in the estimation of its area which may be affected by censoring effects related to the edges of the observation window (this issue is not discussed here). Here, we report a remarkable feature for a BD spot pattern in MIM devices. We have observed that catastrophic BD events generate regions around them that statistically prevent the

appearance of new BD spots in their vicinity. This inhibitory effect seriously questioned the hypothesis of a CSR generation model in case of severely damaged devices.

2. Devices and experimental setup

The MIM devices investigated in this work are square Pt/HfO_2/Pt structures with a 30 nm-thick insulating layer. These capacitors were fabricated on n-type Si (100) substrates with resistivity of 1-4 Ω·cm. Detailed steps about the fabrication process can be found in [2]. For measurements, the bottom electrode was grounded while a constant negative voltage was applied to the top electrode. Constant voltage stress (CVS) around -10V was applied to the device for t=65 s and its progressive degradation image (generation of spots) was recorded using an optical microscope. After the degradation phase, the top electrode surface was inspected by means of a scanning electron microscope (SEM) and by an atomic force microscope (AFM) in order to capture the details of the BD spots. The location and size of the spots were obtained from the videos recorded during the stress using MATLAB routines for image analysis. Subsequently, this information was processed using the Spatstat package for the R language [8].

3. Results and discussion

Figure 2 shows a sequence of photographs (150 μm × 150 μm) corresponding to the degradation process of the top metal layer of a device during the application of a CVS. These images were extracted from a video (see Supplementary Information: video 1). At the beginning, the BD spots appear distributed over the whole device area. However, as the degradation proceeds, burning effects appear on the already damaged electrode. The burned area increases with the stress time. During this phase, a kind of ring develops around the previously generated spots. These rings are not evident before the burning

stage and become visible as the burning effects take place (see arrows 1 and 2). This indicates that some structural modifications occurred in the regions close to the spots that reduce the surface current density around them, reducing in turn the burning effects. Similar effects around the BD spots in MOS transistors were also reported by Cester *et al* [9]. We postulate that the high temperatures reached previously or at the very moment of the local evaporation of the electrode are responsible for remarkable structural changes in the dielectric layer [10]. In order to quantify this observation, a statistical characterization of the BD sites using different estimators was carried out. For the sake of simplicity, the spots and their associated rings are considered as circles with radii r_{spot} and r_{ring}, respectively. The distance between the centers of the spots is also considered and it is referred to as d_{CC} (center-to-center) (see Fig. 3a). In case of spot inhibition in the ring region, the number of spots generated in that region should be much lower than the spots generated in its vicinity (see Fig. 3b).

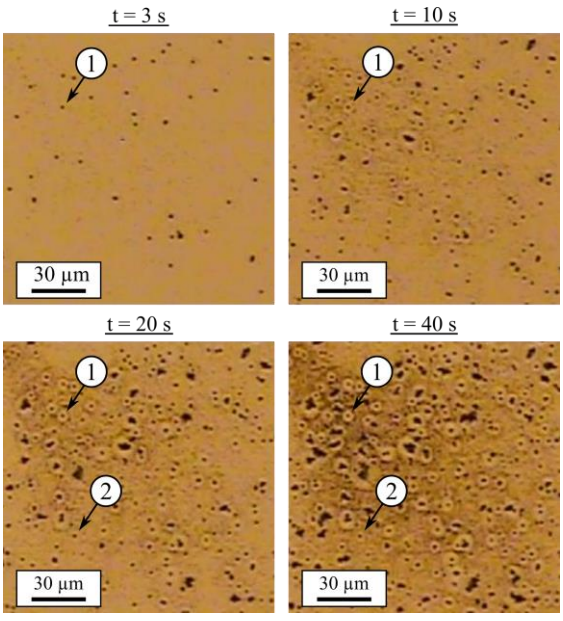

Figure 2. Optical zoom-in images of the top electrode of a Pt/HfO_2/Pt device during the application of -10 V for different degradation times. The size of the images is 150µm × 150µm.

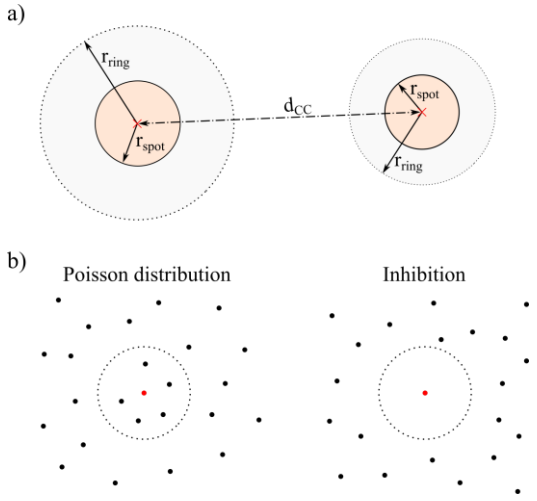

Figure 3. Schematic representation of (a) the distances investigated and (b) the meaning of the inhibitory effect.

Figure 4a shows the distribution of spots for the device illustrated in Fig. 2 after a 15 s stress. The location of the failure sites is shown in Fig. 4b. The spots which are not completely inside the observation window were not considered for the analysis (minus sampling). In Fig. 4c, the empty-space distance map for the region enclosed in dashed line in Fig. 4b is represented. In this plot, the distance from a given pixel to its nearest spot is represented in different colors. A small gap between the spots can be observed. The nearest neighbour function $G(r)$ (see Fig. 4d) evaluates the distance between nearest spots, *i.e.* it gives the cumulative distribution of the distance from a typical point of the distribution to its nearest other point. When compared with a CSR process, the experimental $G(r)$ exhibits lower values for distances shorter than 6 µm than what is theoretically expected. Statistically speaking, this means that the generation of spots in that region is less likely than for a Poisson distribution. In fact, $G(r)$ is zero for distances shorter than 2.7 µm meaning that there are no spots closer than that distance. This is confirmed by the histogram plot for the distance between nearest neighbour spots (Fig. 4e). There are no spots in a distance shorter than 2.5 µm. Importantly, the histogram for

the size of the spots is shown in Fig. 4f. As can be seen, the size of the spots ranges between 0.5 µm and 1.5 µm.

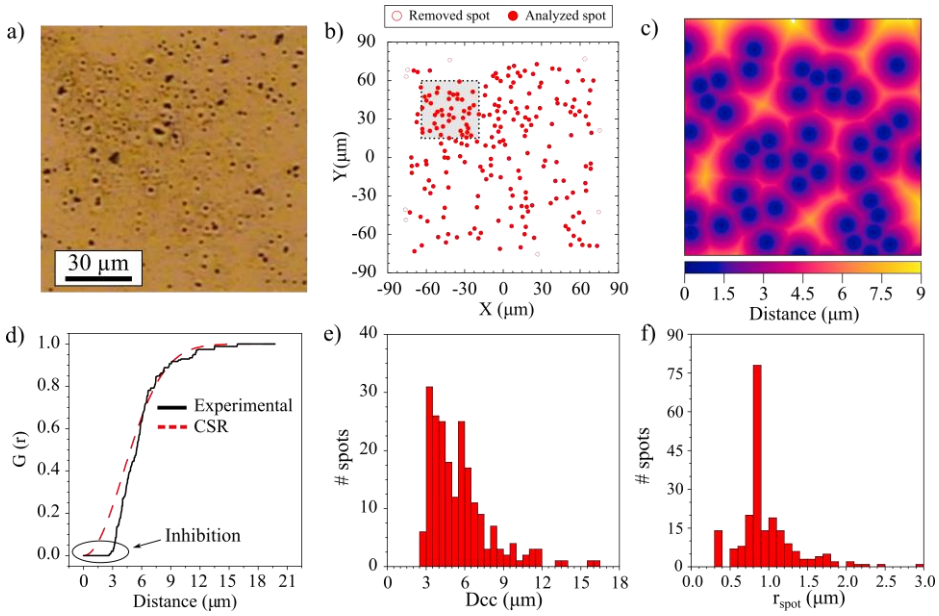

Figure 4. (a) Optical image of the device shown in Fig. 2 after a CVS of 15 s. (b) Location of the spots shown in (a). The spots that are outside the observation window are not considered in the analysis. (c) Empty-space distance map for the region marked in (b). (d) Nearest-neighbour function *G* for the experimental data and for a CSR process. Histogram for (e), the distance between nearest neighbours and (f), the radius of the spots

Figure 5a is a SEM image in which the rings around the spots can be clearly observed. From this image, the size of the rings is obtained. r_{ring} ranges from 2.3 µm to 6.1 µm with an average value of 3.5 µm. Notice that this value is in the range where the distribution in Fig. 3d shows a deficient number of spots (6 µm), supporting the idea that the generation of spots in the ring region is less likely than for a Poisson distribution. This means that some physical modification occurs around the BD spots when they are generated. In order to identify whether there is a deformation of the top metal layer or not, a topographic AFM characterization of the spots was performed (see Fig. 5b). As can be seen, there is no alteration of the metal layer outside the crater-like region, meaning that

the origin of the surface ring might be a consequence of a process that occurred in the dielectric layer and the interaction with the current lines in the top metal layer responsible for the burning effects.

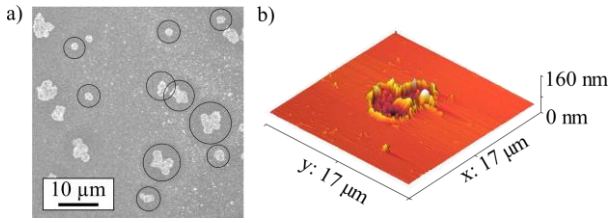

Figure 5. (a) SEM image of the top electrode after the application of a CVS. (b) AFM image of the BD spots showing no alteration of the metal layer outside the crater-like region.

In order to elucidate if the results reported above are only valid for burned devices, a characterization of a BD spot distribution obtained from a non-burned capacitor was carried out (see Fig. 6). In this case, a CVS at -9.5V was applied. Figure 6a shows the distribution of spots obtained on the top electrode after a 65 s stress (see Supplementary information: video 2). In order to compare the results, the same image dimensions were considered (150 µm× 150 µm). The location of the spots shown in Fig. 6a is represented in Fig. 6b. If we pay attention to *G(r)* (Fig. 6c), we observe that there are no BD spots closer than 2.2 µm and that for distances up to 7.2 µm the generation of spots is lower than expected for a CSR distribution. In this case, the inhibition distance is also found to be in the range of the ring size. Notice that the ring is not observed as the device does not exhibit burning effects. Finally, in Fig. 6d the histogram for the size of the spots is illustrated. The size of the spots ranges from 0.5 µm to 0.8 µm, which is a range lower than previously found (Fig. 4f). We surmise that this is a consequence of using a lower stress voltage.

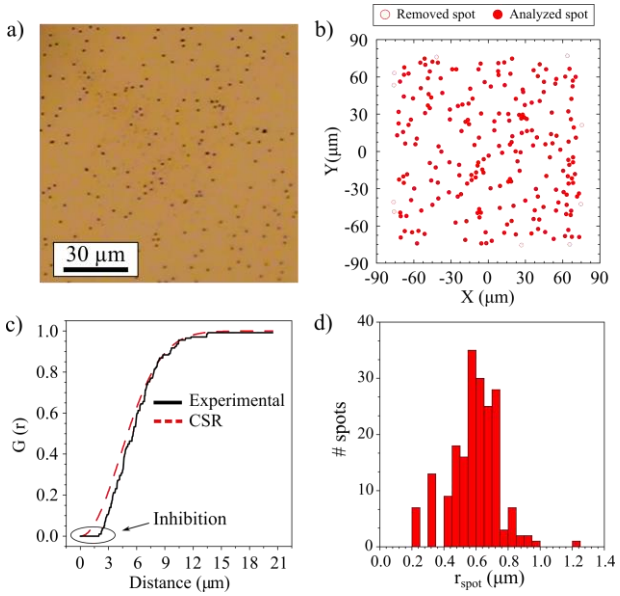

Figure 6. (a) Optical zoom-in image of a device after a CVS of 65 s. The size of the image is 150µm × 150µm. (b) Location of the spots shown in (a). The spots that are outside the observation window are not considered in the analysis. (c) Nearest-neighbour function *G* for the experimental data and for a CSR process. (d) Histogram for the radius of the spots.

4. Conclusions

In this paper, the generation of soft-inhibition regions around catastrophic BD spots is reported for Pt/HfO_2/Pt devices. This observation seriously questions the CSR hypothesis for the generation of spots, at least for severely damaged devices. It seems that the inhibitory effect arises from a structural modification of the dielectric film in the vicinity of the spot caused by the huge thermal effects that occur during the breakdown phase. The effect only becomes observable when burning effects appear in the degraded metal electrode.

Acknowledgements

The authors acknowledge project TEC2017-84321-C4-4-R, MINECO, Spain.

References

[1] A. S. Oates, "Reliability issues for high-k gate dielectrics," in *IEEE International Electron Devices Meeting (IEDM)*, pp. 923–926, 2003.

[2] J. Muñoz-Gorriz, S. Monaghan, K. Cherkaoui, J. Suñé, P. K. Hurley, and E. Miranda, "Exploratory study and application of the angular wavelet analysis for assessing the spatial distribution of breakdown spots in Pt/HfO_2/Pt structures," *J. Appl. Phys.*, vol. 122, no. 21, p. 215304, 2017.

[3] E. Y. Wu, J. H. Stathis, and L.-K. K. Han, "Ultra-thin oxide reliability for ULSI applications," *Semicond. Sci. Technol.*, vol. 15, no. 5, pp. 425–435, May 2000.

[4] J. Muñoz-Gorriz, S. Monaghan, K. Cherkaoui, J. Suñé, P. K. Hurley, and E. Miranda, "Characterization of the Failure Site Distribution in MIM Devices Using Zoomed Wavelet Analysis," *J. Electron. Mater.*, vol. 47, no. 9, pp. 5033–5038, 2018.

[5] S. Claramunt, Q. Wu, M. Maestro, M. Porti, M. B. Gonzalez, J. Martin-Martinez, F. Campabadal, M. Nafria, "Non-homogeneous conduction of conductive filaments in Ni/HfO_2/Si resistive switching structures observed with CAFM," *Microelectron. Eng.*, vol. 147, pp. 335–338, 2015.

[6] A. Baddeley, E. Rubak, and R. Turner, *Spatial point patterns : methodology and applications with R*. Chapman and Hall/CRC, 2015.

[7] J. Illian, A. Penttinen, H. Stoyan, D. Stoyan, *Statistical Analysis and Modelling of Spatial Point Patterns*, vol. 47, no. 4. Chichester, UK: John Wiley & Sons, Ltd, 2005.

[8] A. Baddeley and R. Turner, "spatstat : An R Package for Analyzing Spatial Point Patterns," *J. Stat. Softw.*, vol. 12, no. 6, 2005.

[9] A. Cester, A. Paccagnella, G. Ghidini, S. Deleonibus, and G. Guegan, "Collapse of

MOSFET Drain Current After Soft Breakdown," *IEEE Trans. Device Mater. Reliab.*, vol. 4, no. 1, pp. 63–72, Mar. 2004.

[10] S. Kumar, Z. Wang, X. Huang, N. Kumari, N. Davila, J. P. Strachan, D. Vine, A. L. D. Kilcoyne, Y. Nishi, R. S. Williams, "Oxygen migration during resistance switching and failure of hafnium oxide memristors," *Appl. Phys. Lett.*, vol. 110, no. 10, p. 103503, 2017.